Kinetics of plasma flowing around two stationary dust grains

S. V. Vladimirov,* S. A. Maiorov,† and N. F. Cramer
School of Physics, The University of Sydney, New South Wales 2006, Australia
(Received 19 March 2002; revised manuscript received 17 September 2002; published 29 January 2003)

The characteristics of plasma particle kinetics in the presence of ions flowing around two stationary dust grains aligned in the direction of the flow are studied using a three-dimensional molecular dynamics simulation code. The dynamics of plasma electrons and ions as well as the charging process of the dust grain are simulated self-consistently. Distributions of electron and ion number densities, and the electrostatic plasma potential are obtained for various intergrain distances, including those much less, of the order of, and more than the plasma electron Debye length.

DOI: 10.1103/PhysRevE.67.016407 PACS number(s): 52.27.Lw, 52.25.Vy, 52.35.Fp, 52.40.Hf

I. INTRODUCTION

The fundamental question of importance for the understanding of processes involving the formation and evolution of various self-organized structures such as colloidal crystals [1] and other formations like dust clouds, dust voids, etc. [2–6] in a complex ''dusty'' plasma, is the interaction of dust grains with themselves and the surrounding plasma. Since in a typical laboratory discharge dust particles are negatively charged and usually levitate in the sheath or presheath region under the balance of gravitational, electrostatic, (due to the sheath electric field) and plasma (such as the ion drag) forces, these interactions involve collective processes associated with the flowing plasma. The ion flow, providing a direct dragging influence (supporting, in particular, the formation of dust voids [3,4]), is also responsible for the generation of associated collective plasma processes such as the formation of the plasma wake [7–13]. The latter can strongly modify the interactions of dust grains between themselves and with the plasma, in particular, supporting a Cooper-pairing-like attraction of grains of the same sign of the charge [7,14]. The complete problem of plasma dynamics around a macroscopic body in the presence of plasma flows is highly nonlinear and therefore its numerical analysis is of major importance. Various numerical methods can be employed to solve the problem. Among them, direct integration of the equations of motions of plasma particles represents a numerical experiment with significance approaching experiments in the laboratory.

The problem of plasma kinetics in the presence of a macroscopic body is also connected to the charging of the body. For a typical situation of a low-temperature laboratory dusty plasma, the macroparticle charge appears as a result of charging plasma currents onto the particle surface [15]. Several models of particle charging were developed, the orbit-limited theory (OLM) being the basic one [16]. Also, a number of experiments [17–21] have been performed to elucidate the character of the charge of an isolated particle; most of experimental techniques are complicated, requiring special measurement procedures and, on the other hand, do not always give the precise results. Moreover, it is especially difficult to determine the particle charges for *two* particles, especially in the sheath region in the presence of the ion flow. In this case, the *ab initio* numerical simulation, being one of the most complete model description, can provide very important information on the character of the plasma kinetics and particles' charging.

The modeling of the plasma response to the presence of colloidal dust particles in the presence of plasma flows is usually performed by particle-in-cell methods [22,23]. The first report on the self-consistent three-dimensional molecular dynamics simulation [24] of plasma kinetics around one stationary dust grain demonstrated strong ion focusing, with the ion density in the focus exceeding the ion density in the flow by a factor of 5–6. Thus, the charging of the second dust grain located behind the first one, will be strongly affected by this (highly nonlinear) effect. On the other hand, the plasma dynamics around and behind the second macroscopic body is a function of its charge and, therefore, the full self-consistent simulation of such an arrangement should necessarily take into account the charging of the second dust particle in the wake of the first one. It is natural to expect that the charge of this second particle will, therefore, differ from the charge of the first particle. Here, we note that the anisotropy of the forces appearing, e.g., in two-dimensional chains, is important for the proper modeling of processes in these structures levitating in the flow [25,26], also, the ion charge accumulated behind dust grains, associated with the plasma wake, can also drive some instabilities in the dust chains [27]; on the other hand, the analytical modeling can hardly provide the relevant number because of the high nonlinearity of the processes involved.

Here, we present the results of a self-consistent molecular dynamics (MD) three-dimensional simulation of the kinetics of plasma electrons and ions around two aligned (in the direction of the flow) dust grains, taking into account the dust charging and the supersonic ion flow. We present the simulated distributions of plasma electron and ion densities as well as of the plasma potential. The charges of the grains are calculated self-consistently, and their values for different distances between the grains are presented.

*Email address: S.Vladimirov@physics.usyd.edu.au;
URL: http://www.physics.usyd.edu.au/~vladimi
†Permanent address: Department of Theoretical Physics, General Physics Institute, Moscow 117942, Russia.

TABLE I. The intial values for the dust grain and plasma particles. $m_p = 1842 m_e$ is the proton mass, $m_e = 9.11 \times 10^{28}$ g is the electron mass, and $e = 4.8 \times 10^{-10}$ statcoul is the (absolute) electron charge (where n/a denotes data not applicable).

	Macroparticles	Ions	Electrons
Charge	$1250e$	$-e$	e
Mass	∞	$4m_p$	$100m_e$
Number	1	5000	2500
Temperature	n/a	0.025 eV	1 eV

II. NUMERICAL PROCEDURE

The details of the technique used for the numerical integration of the equations of multiparticle dynamics are described in [24,28]. The numerical method used involves simulation of the time evolution of the fully ionized ($Z_i = 1$, i.e., the ions are single charged) plasma consisting of N_i positively (ions) and N_e negatively (electrons) charged particles confined in a simulation box $0 < x < L_x$, $0 < y < L_y$, $0 < z < L_z$, together with two macroscopic absorbing grains (dust particles), each of radius $R = 0.5$ μm, with infinite masses and initial (negative) charges $Q_{1,2} = Z_{d1,2}e$, where e is the electron charge. The details are given in Table I.

Although in the computational model the electron mass is assumed to be $100m_e$, see Table I, we note that when simulating the charging process, we effectively take into account the real electron/ion mass ratio by renormalizing the electron current and therefore the absorbed charge in the process of the electron-dust charging collision, so that the charge appearing on the grain corresponds to its value for the real electron/ion mass ratio, see for details [24]. In the simulation, the ion number density was calculated by averaging within the spherical layer around the macroparticle. The results for an isolated particle in the presence as well as in the absence of the ion flow demonstrate good agreement with the analytical OLM results [24].

The ions are introduced in the system at the plane $x = 0$ as a uniform flow in the x direction with the Mach number $M = V_0/V_s (V_0 > 0)$ and the temperature T_i, where $V_s = (T_e/m_i)^{1/2}$ is the speed of the collisionless sound waves, T_e is the temperature of plasma electrons (all temperatures are in energy units, i.e., Boltzmann's constant is unity), and m_i is the ion mass; at $x = L_x$ the ions are removed from the system. The walls bounding the simulation region are elastic for electrons; for ions, they are elastic in the y and z directions, i.e., at $y = (0, L_y)$ and $z = (0, L_z)$. This means that electrons are specularly reflected from the walls in all directions, on the other hand, since the ions are moving in the x direction, for them the specular reflection condition applies in the y and z directions.

The total number of electrons and total number of ions in the system is fixed; it is chosen on the basis of test simulation runs to satisfy the given number densities and to make sure that the system is neutral as a time average. In the place of the ion absorbed by the dust grains (or at the back wall of the simulation box), a new one is introduced at a random point on the front wall with the chosen velocity distribution function (the latter is assumed to be shifted Maxwellian). The dust grains are placed at $x = x_0 = L_x/4$ and $x = x_0 + D$, such that D is the distance between the grains, with the other coordinates being $y = y_0 = L_y/2$ and $z = z_0 = L_z/2$; thus, the grains are aligned in the direction parallel to the ion flow.

TABLE II. The charges on the dust grains depending on the distance between them.

Distance D	Charge Q_1	Charge Q_2
$0.06L_x = 0.25\lambda_{De}$	1390	840
$0.10L_x = 0.41\lambda_{De}$	1420	860
$0.15L_x = 0.62\lambda_{De}$	1390	840
$0.20L_x = 0.82\lambda_{De}$	1430	1010
$0.25L_x = 1.03\lambda_{De}$	1470	1040
$0.35L_x = 1.45\lambda_{De}$	1500	1080
$0.40L_x = 1.64\lambda_{De}$	1410	1020
$0.50L_x = 2.05\lambda_{De}$	1480	1130
$0.60L_x = 2.46\lambda_{De}$	1450	1230
$0.65L_x = 2.67\lambda_{De}$	1430	1180
$1.00L_x = 4.10\lambda_{De}$	1460	1200
∞	1450	n/a

The initial distributions of the coordinates of plasma electrons and ions is chosen to be homogeneous within the simulation box, the initial velocity distributions correspond to Maxwellian for electrons and shifted Maxwellian for ions at infinity. Depending on the distance to the colloidal particles, the distributions are distorted because of the interactions with the macroparticles. Thus, the initial distributions do not include finite ion orbits which can strongly affect the kinetic characteristics under certain circumstances [29].

The trajectories of the plasma electrons and ions are determined through numerical integration of the equations of motion

$$\frac{d^2\mathbf{r}_k}{dt^2} = \frac{\mathbf{F}_k}{m_k}, \tag{1}$$

where $\mathbf{F}_k = \Sigma_1^{1+N_i+N_e} \mathbf{f}_{kl}$ and the Coulomb force is given by $\mathbf{f}_{kl} = q_k q_l \mathbf{r}_{kl} / |\mathbf{r}_{kl}|^3$. For the Coulomb force at very small distances, we used the corresponding expression for finite (small) size mutually penetrating spheres [28].

The equations of motion are solved by the Runge-Kutta method of the fourth order with an automatically chosen time step. For the characteristic lengths, we have (for most calculations unless otherwise specified) $L_x/2 = L_y = L_z = 20h_x$ with the spacing $h_x = 2h_y = 2h_z = 0.5375$ μm. For the given values, the characteristic lengths in the plasma are: electron Debye length $\lambda_{De} = 5.256$ μm and ion Debye length $r_{Di} = 0.831$ μm. The ion number density is $n_i = 2 \times 10^{12}$ cm^{-3}, and hence the ion Debye length in term of the average ion-ion distance $r_{Di} n_i^{1/3} = 1.06$; the number of ions in the ion Debye sphere is ≈ 5. Note than since the ions are supersonic, their energy exceeds T_e and they are really weakly coupled. For electrons, we have $r_{De} n_e^{1/3} = 5.25$ that corresponds to

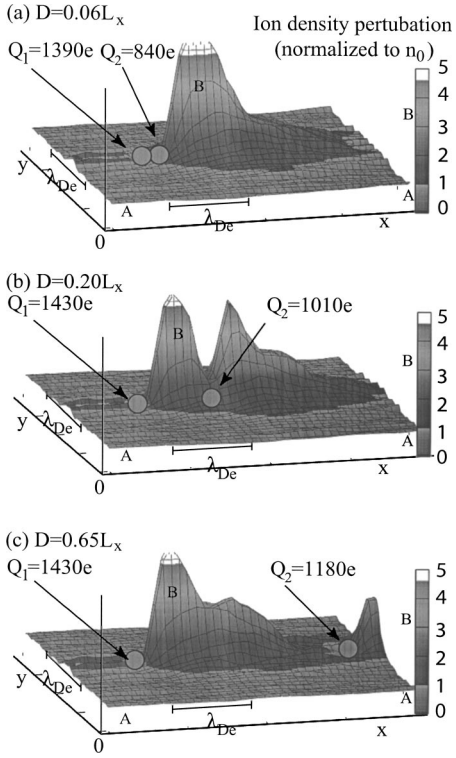

FIG. 1. Surface plot of the normalized ion density, showing ion focusing, for three different separations D between two dust grains. The plot is presented in the greyscale topograph style; regions A correspond to the normalized (to the unperturbed ion density n_{i0}) ion densities below 1, and regions B correspond to the normalized ion densities above 1. The distances are given in the units of the total length of the simulation box in the direction of the ion flow $L_x \approx 4.1\lambda_{De}$ used in the calculation; the physical distance corresponding to the electron Debye length λ_{De} is also presented.

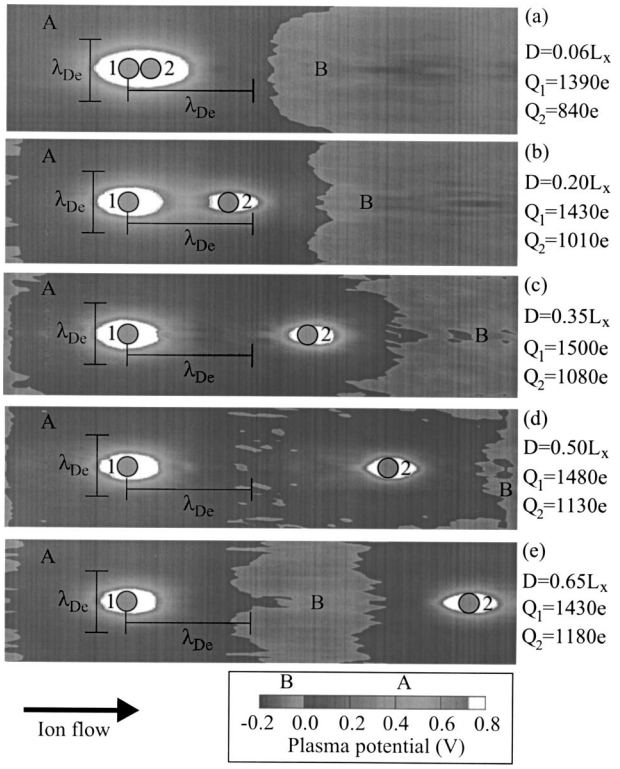

FIG. 2. Contour plot of the plasma potential for five different distances between two dust grains. The plot is presented in the greyscale topograph style. Note that the potential well (region B) is formed behind the dust grain and starts to form between the grains when the separation exceeds the electron Debye length.

more than 500 electrons in the electron Debye sphere, and we can consider the system as an ideal plasma. Finally, the electron and ion number densities are chosen to be higher than those in real experiments for numerical reasons (to decrease the plasma Debye length).

The total simulated time of the physical processes is 9.2×10^{-9} s, which should be compared with the inverse ion plasma frequency $\tau_{pi} = 1/\omega_{pi} = 3.4 \times 10^{-9}$ s. The time step of the numerical simulation is 4×10^{-12} s which is not only much less than the inverse ion plasma frequency, but is also much less than the electron plasma frequency $\tau_{pe} = 1/\omega_{pe} = 8 \times 10^{-10}$ s. The speed of the ion flow corresponds to the Mach number $M = 2$. The Landau length for scattering of the ions on the dust particle by the angle $\pi/2$ is $r_L \equiv Z_d e^2/m_i V_0^2$, for our parameters $r_L \approx 0.5$ μm (for the dimensionless charge $Z_d = 1400$).

III. SIMULATION RESULTS

Table II demonstrates the dependence of the charges accumulated on the dust grains as functions of the intergrain distance. We see that when the particles are very close to each other, their charges are influenced by the presence of the other particle. This influence is especially strong for the second (i.e., downstream) particle; its charge is significantly (typically, 40%) less than the charge of an isolated particle (see the last line of the table). As soon as the distance between the particles is increased, the second charge exhibits a noticeable increase; it is interesting to note that the first charge is increased, too, although by a lesser value. We also see that when the interparticle separation exceeds the electron Debye length ($D = 1.03\lambda_{De} - 1.45\lambda_{De}$), the increase of the charge of the first-particle stops, on the other hand, the increase of the charge accumulated on the second particle located downstream continues to grow until the distance ex-

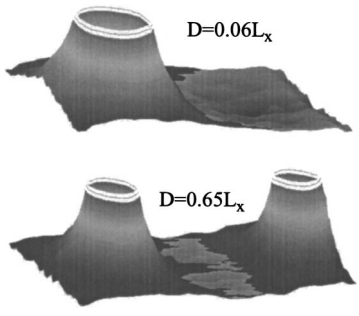

FIG. 3. Surface plot of the plasma potential for two different velocities distances between the dust grains (much less than the electron Debye length and more than the electron Debye length). The potential well due to the wake is formed on the distance of the order of the electron Debye length behind the grain(s).

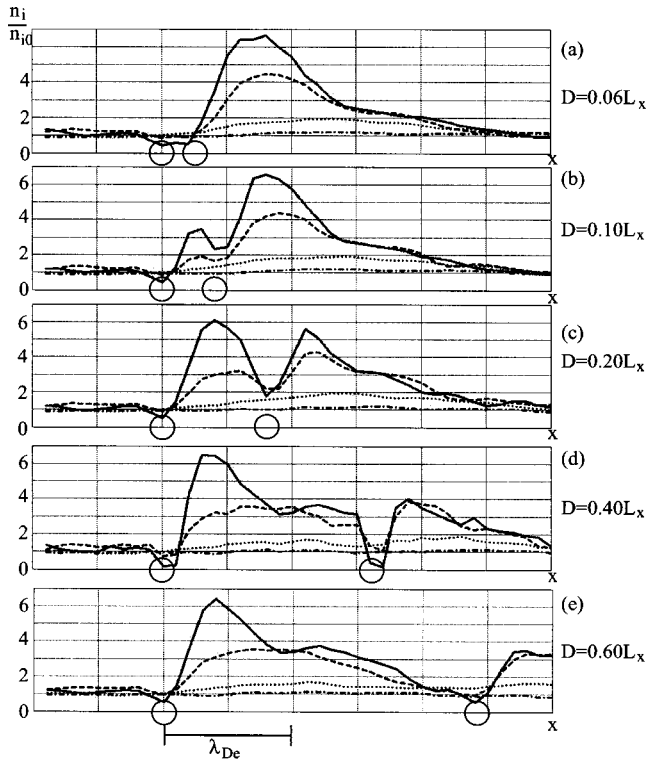

FIG. 4. The distribution of the normalized ion density parallel to the ion flow, for four lines: $y=5.4h_y$ (solid curve, corresponds to the middle of the simulation box in y direction), $y=5.7h_y$ (dashed curve, corresponds to the distance of $0.06\lambda_{De}$ from the middle of the simulation box in y direction), $y=6.4h_y$ (dotted curve, corresponds to the distance of $0.20\lambda_{De}$ from the middle of the simulation box in y direction), and $y=7.8h_y$ (dash-dotted curve, corresponds to the distance of $0.46\lambda_{De}$ from the middle of the simulation box in y direction). Five different distances between two dust grains are presented as well as the distance corresponding to the electron Debye length in the direction x parallel to the ion flow.

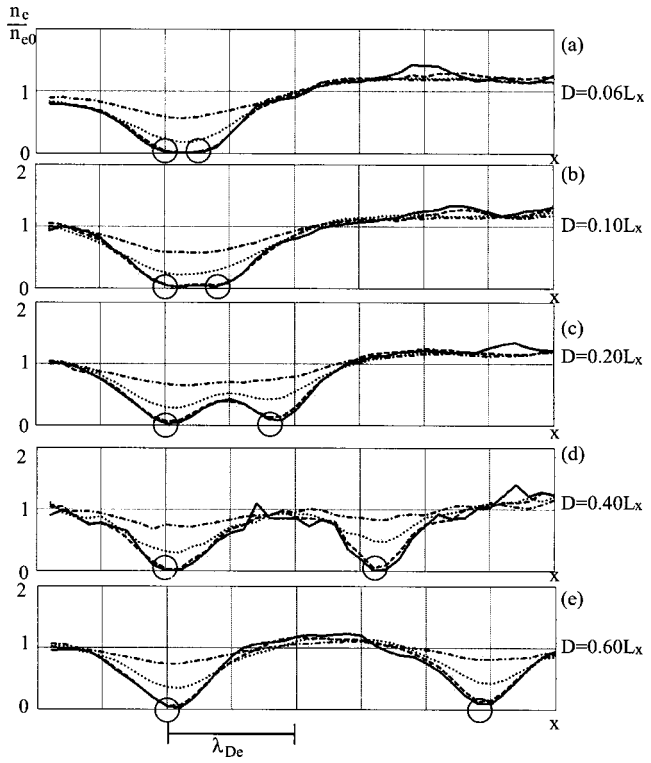

FIG. 5. The distribution of the normalized electron density parallel to the ion flow, for four lines: $y=5.4h_y$ (solid curve, corresponds to the middle of the simulation box in y direction), $y=5.7h_y$ (dashed curve, corresponds to the distance of $0.06\lambda_{De}$ from the middle of the simulation box in y direction), $y=6.4h_y$ (dotted curve, corresponds to the distance of $0.20\lambda_{De}$ from the middle of the simulation box in y direction), and $y=7.8h_y$ (dash-dotted curve, corresponds to the distance of $0.46\lambda_{De}$ from the middle of the simulation box in y direction). Five different distances between two dust grains are presented as well as the distance corresponding to the electron Debye length in the direction x parallel to the ion flow.

ceeds two electron Debye lengths ($D=2.46\lambda_{De}$). We can attribute this phenomenon to the fact that the ion wake of the first particle is spreading at distances significantly exceeding the electron Debye length, on the other hand, the influence of the second (i.e., downstream) particle on the charge of the first one in the simplest approximation is limited to distances of the order of the electron Debye length. Note that other charge variations express fluctuations always present in the particle charges as well as the plasma parameters, see also [23]. Another interesting phenomenon is that the charge of the second particle, at the considered distances (up to $D=4.1\lambda_{De}$), is always less than the charge of the first particle, thus confirming the long-range influence of the ion wake.

To compare the results for two particles with the case of an isolated particle, we present in the last line of Table II the result of the special simulation run for the charge of the first particle when the second particle is removed from the system ($D=\infty$). The particle charge in this case ($Q=1450e$) coincides with other numerical MD [24] as well as particle-in-cell (PIC) [23] simulations, moreover, this result also agrees to the model OLM calculation for a particle levitating in the sheath region in the presence of the ion flow [30].

In Fig. 1, we present surface plots of the ion density n_i normalized to $n_{i0}=N_i/L_xL_yL_z$, for three different distances between the charged colloidal particles: the first one [Fig. 1(a)] corresponds to the short distance of $D=0.25\lambda_{De}$, the second one [Fig. 1(b)] is of the order of the electron Debye length: $D=0.82\lambda_{De}$, and the third one [Fig. 1(c)] corresponds to the relatively large distance exceeding the electron Debye length: $D=2.7\lambda_{De}$. For better visualization, parts of the simulation volume where $n_i/n_{i0}<1$ and $n_i/n_{i0}>1$, respectively, are presented in the (greyscale) topograph style, i.e., part A is for $n_i/n_{i0}<1$ and part B is for $n_i/n_{i0}>1$, so that the change from lower (with respect to n_{i0}) to higher densities is clearly seen. A strong ion focus is formed at the distance of a fraction of the electron Debye length behind the first dust grain; depending on the position of the second grain, the wake maximums are either combined, see Fig. 1(a), or clearly separated, see Fig. 1(c).

Figure 2 gives the contour plot of the plasma potential (in V) for five different distances between the grains: (a) corresponds to a short distance which is much less than the electron Debye length, $D=0.25\lambda_{De}$, (b) is for the increased distance $D=0.82\lambda_{De}$, (c) is for $D=1.43\lambda_{De}$, (d) is for D

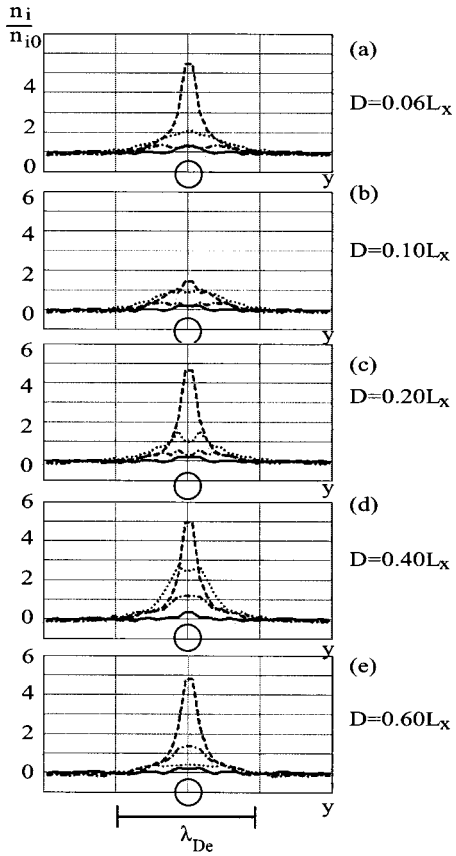

FIG. 6. The distribution of the normalized ion density perpendicular to the ion flow, for four lines: $x=0$ (solid curve, corresponds to the left wall of the simulation box in x direction and to the distance $1.05\lambda_{De}$ before the center of the first grain, i.e., in the upstream direction), $x=8.1h_x$ (dashed curve, corresponds to the distance of $0.5\lambda_{De}$ after the center of the first grain, i.e., in the downstream direction), $x=16.1h_x$ (dotted curve, corresponds to the distance of $2.05\lambda_{De}$ after the center of the first grain, i.e., in the downstream direction), and $x=19.4h_x$ (dash-dotted curve, corresponds to the distance of $2.66\lambda_{De}$ after the center of the first grain, i.e., in the downstream direction). Five different distances between two dust grains are presented as well as the distance corresponding to the electron Debye length in the direction y perpendicular to the ion flow.

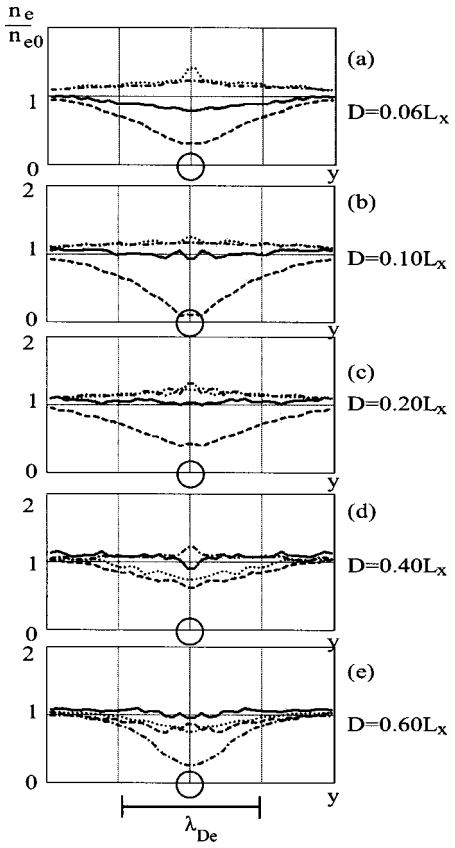

FIG. 7. The distribution of the normalized electron density perpendicular to the ion flow, for four lines: $x=0$ (solid curve, corresponds to the left wall of the simulation box in x direction and to the distance $1.05\lambda_{De}$ before the center of the first grain, i.e., in the upstream direction), $x=8.1h_x$ (dashed curve, corresponds to the distance of $0.5\lambda_{De}$ after the center of the first grain, i.e., in the downstream direction), $x=16.1h_x$ (dotted curve, corresponds to the distance of $2.05\lambda_{De}$ after the center of the first grain, i.e., in the downstream direction), and $x=19.4h_x$ (dash-dotted curve, corresponds to the distance of $2.66\lambda_{De}$ after the center of the first grain, i.e., in the downstream direction). Compare with Fig. 6.

$=2.1\lambda_{De}$, and (e) is for a distance relatively large with respect to the electron Debye length $D=2.7\lambda_{De}$. We see that for short distances [Figs. 2(a) and 2(b)], the wake is practically corresponding to that of one combined particle; on the other hand, for distances of the order of, Fig. 2(d), or more than, Fig. 2(e), the electron Debye length, the formation of quasiwake features can be seen after the first grain, i.e., before the second one. The characteristic distance for the region of the attractive potential to appear in the x direction is of the order of the electron Debye length, thus, coinciding with the linear theory [7]. The three-dimensional surface plot of the plasma potential is presented in Fig. 3, for two distances: (a) is for a distance which is much less than the electron Debye length $D=0.25\lambda_{De}$ [see also Fig. 2(a)], and (b) is for a distance which is more than the electron Debye length $D=2.7\lambda_{De}$ [see also Fig. 2(e)].

In Fig. 4, we present the cross sections of the normalized ion density in the direction parallel to the ion flow. For better visualizing of the scale, we also plot the grain size (circle). Five different distances between the grains are presented: (a) $D=0.25\lambda_{De}$, (b) $D=0.41\lambda_{De}$, (c) $D=0.82\lambda_{De}$, (d) $1.64\lambda_{De}$, and (e) $D=2.45\lambda_{De}$. Note that here, we have presented more cases for distances less than and of the order of the electron Debye length. We plot four curves corresponding to $z=L_z/2$ and: (1) $y=5.4h_y=L_y/2$ (solid curve). This line is parallel to x and is in the middle of the simulation box in y direction, and it crosses the centers of the grains; (2) $y=5.7h_y$ (dashed curve). This line is at the distance $0.06\lambda_{De}$ from the centers of the grains in the direction perpendicular to the flow (y); (3) $y=6.4h_y$ (dotted curve). This line is at the distance $0.20\lambda_{De}$ from the centers of the grains in the direction perpendicular to the flow (y); and (4) $y=7.8h_y$ (dash-dotted curve). This line is at the distance $0.46\lambda_{De}$ from the centers of the grains in the direction perpendicular to the flow (y). We see that the major maximums of the ion den-

sities in the wake are typically formed at distances of a fraction of the electron Debye length. Figure 5 presents the cross sections of the electron density normalized to $n_{e0} = N_e / L_x L_y L_z$, in the direction parallel to the ion flow. Other parameters and curves are the same as in Fig. 4. Here, we see that the electron screening length corresponds to the electron Debye length; also, distortions of the electron density appear behind the grains at a distance of the order of the electron Debye length due to the plasma wake formation, as shown also by the plasma potential in Figs. 2 and 3.

Finally, Figs. 6 and 7 present the cross sections of the normalized ion (Fig. 6) and electron (Fig. 7) densities in the direction perpendicular to the ion flow; the distances between the grains are the same as in Figs. 4 and 5, (a)–(e), and four curves are presented ($z = L_z/2$): (1) $x = 0$ (solid curve). This line corresponds to the left wall of the simulation box (where the ion flow is introduced in the system), and it is at the distance $1.05\lambda_{De}$ from the center of the first grain in the upstream (with respect to the ion flow) direction; (2) $x = 8.1h_x$ (dashed curve). This line is at the distance $0.5\lambda_{De}$ from the center of the first grain in the direction downstream with respect to the ion flow; (3) $x = 16.1h_x$ (dotted curve). This line is at the distance $2.05\lambda_{De}$ from the center of the first grain in the direction downstream with respect to the ion flow; and finally, (4) $x = 19.4h_x$ (dash-dotted curve). This line is at the distance $2.66\lambda_{De}$ from the center of the first grain in the direction downstream with respect to the ion flow.

IV. CONCLUSION

To conclude, we have self-consistently simulated from first principles by MD calculations the plasma kinetics around two charged macroscopic bodies (dust grains) in the presence of an ion flow (and therefore involving strong ion focusing behind the grains). We have demonstrated that the ion wake strongly influences the charge of the second grain located downstream with respect to the first particle. This influence is especially strong for intergrain distances small compared to the electron Debye length. It is interesting that there is also an influence of the downstream particle on the charge of the particle located upstream; this influence, however, is limited to distances of the order of the electron Debye length, in agreement with the Debye approximation. The charge of the second particle, for the distances considered (up to four electron Debye lengths), is always less than the charge of the first particle, and this is attributed to the long-range influence of the plasma wake. The simulated plasma electron and ion densities as well as their cross sections provide details of the corresponding distributions within and outside the wake.

ACKNOWLEDGMENTS

This work was supported by the Australian Research Council.

[1] H.M. Thomas and G.E. Morfill, Nature (London) **379**, 806 (1996).
[2] D. Samsonov and J. Goree, Phys. Rev. E **59**, 1047 (1999).
[3] J. Goree, G.E. Morfill, V.N. Tsytovich, and S.V. Vladimirov, Phys. Rev. E **59**, 7055 (1999).
[4] V.N. Tsytovich, S.V. Vladimirov, G.E. Morfill, and J. Goree, Phys. Rev. E **63**, 056609 (2001).
[5] G.E. Morfill, H.M. Thomas, U. Konopka, H. Rothermel, M. Zuzic, A. Ivlev, and J. Goree, Phys. Rev. Lett. **83**, 1598 (1999).
[6] V.N. Tsytovich, S.V. Vladimirov, and S. Benkadda, Phys. Plasmas **6**, 2972 (1999).
[7] S.V. Vladimirov and M. Nambu, Phys. Rev. E **52**, 2172 (1995).
[8] F. Melandso and J. Goree, Phys. Rev. E **52**, 5312 (1995).
[9] S.V. Vladimirov and O. Ishihara, Phys. Plasmas **3**, 444 (1996).
[10] V.A. Schweigert, I.V. Schweigert, A. Melzer, A. Homann, and A. Piel, Phys. Rev. E **54**, 4155 (1996).
[11] O. Ishihara and S.V. Vladimirov, Phys. Plasmas **4**, 69 (1997); Phys. Rev. E **57**, 3392 (1998).
[12] S. Benkadda, V.N. Tsytovich, and S.V. Vladimirov, Phys. Rev. E **60**, 4708 (1999).
[13] M. Lampe, G. Joyce, G. Ganguli, and V. Gavrishchaka, Phys. Plasmas **7**, 3851 (2000).
[14] K. Takahashi, T. Oishi, K. Shimonai, Y. Hayashi, and S. Nishino, Phys. Rev. E **58**, 7805 (1998).
[15] E.C. Whipple, Rep. Prog. Phys. **44**, 1198 (1981).
[16] J. Goree, Plasma Sources Sci. Technol. **3**, 400 (1994).
[17] S. Peters, A. Homann, A. Melzer, and A. Piel, Phys. Lett. A **223**, 389 (1996).
[18] A. Homann, A. Melzer, and A. Piel, Phys. Rev. E **59**, R3835 (1999).
[19] U. Konopka, L. Ratke, and H.M. Thomas, Phys. Rev. Lett. **79**, 1269 (1997).
[20] E.B. Tomme, D.A. Law, B.M. Annaratone, and J.E. Allen, Phys. Rev. Lett. **85**, 2518 (2000).
[21] V.E. Fortov, A.P. Nefedov, V.I. Molotkov, M.Y. Poustylnik, and V.M. Torchinsky, Phys. Rev. Lett. **87**, 205002 (2001).
[22] D. Winske, W. Daughton, D.S. Lemmons, and M.S. Murillo, Phys. Plasmas **7**, 2320 (2000).
[23] S.V. Vladimirov, S.A. Maiorov, and N.F. Cramer, Phys. Rev. E **63**, 045401 (2001).
[24] S.A. Maiorov, S.V. Vladimirov, and N.F. Cramer, Phys. Rev. E **63**, 017401 (2001).
[25] S.V. Vladimirov, P.V. Shevchenko, and N.F. Cramer, Phys. Plasmas **5**, 4 (1998).
[26] S.V. Vladimirov and A.A. Samarian, Phys. Rev. E **65**, 046416 (2002).
[27] A.V. Ivlev and G.E. Morfill, Phys. Rev. E **63**, 016409 (2001).
[28] R. W. Hockney and J. W. Eastwood, *Computer Simulation Using Particles* (McGraw-Hill, New York, 1981).
[29] M. Lampe, V. Gavrishchaka, G. Ganguli, and G. Joyce, Phys. Rev. Lett. **86**, 5278 (2001).
[30] S.V. Vladimirov, N.F. Cramer, and P.V. Shevchenko, Phys. Rev. E **60**, 7369 (1999).